Full-Scale Laboratory Evaluation of Hybrid Composite Beams for Implementation in a Virginia Bridge

http://www.virginiadot.org/vtrc/main/online_reports/pdf/19-r3.pdf

CRISTOPHER D. MOEN, Ph.D., P.E.
CEO and President
NBM Technologies, Inc.

CARIN L. ROBERTS-WOLLMANN, Ph.D., P.E.
Professor
The Charles E. Via, Jr. Department of Civil and Environmental Engineering
Virginia Polytechnic Institute and State University

THOMAS E. COUSINS, Ph.D., P.E.
Professor
Glenn Department of Civil Engineering
Clemson University

Final Report VTRC 19-R3

Title:

Full-Scale Laboratory Evaluation of Hybrid Composite Beams for Implementation in a Virginia Bridge

Author(s):

Cristopher D. Moen, Ph.D., P.E., Carin L. Roberts-Wollmann, Ph.D., P.E., and Thomas E. Cousins, Ph.D., P.E.

Performing Organization Name and Address:

The Charles E. Via, Jr. Department of Civil and Environmental Engineering
Virginia Polytechnic Institute and State University
Blacksburg, VA

Abstract:

This research project studied a steel-reinforced concrete and fiber-reinforced polymer (FRP) structural element called the Hybrid-Composite Beam (HCB). The beam was used in a skewed simple span superstructure replacement project over the Tides Mill Stream in Colonial Beach, Virginia. For typical HCB construction, each beam is transported to site as a lightweight FRP beam shell. Self-consolidating concrete is pumped into the shell interior arch form, and when the concrete hardens, it stiffens and strengthens the beam so that it can act as falsework to carry the weight of a cast-in-place concrete bridge deck. Unstressed prestressing strands are embedded in the FRP shell bottom flange during the resin placement, and these strands equilibrate thrust in the arch and stiffen the beam to meet service deflection criteria. After the deck is placed, the HCB system performs as a longitudinal flexural member, with the bridge deck resisting compression and prestressing strands and the FRP bottom flange resisting tension.

The primary research goal was to document the HCB as a structural component and as a bridge system, with the outcome being validation of key assumptions that can be applied to future designs such as, for example, strain compatibility between the FRP shell and steel strands. The research was conducted in five phases. In Phase 1, the HCB flexural rigidity and through-depth strain distributions were quantified considering just the FRP shell with unstressed strands. These tests confirmed flexural rigidity estimated by hand calculations and strain compatibility under uniform loads. Phase 2 evaluated flexural behavior of the HCB FRP shell and poured concrete arch. Phase 3 testing was performed after three HCBs were made integral with cast-in-place concrete end diaphragms and a reinforced concrete bridge deck. Point loads, to simulate an HL-93 design truck as specified in American Association of State Highway and Transportation Officials (AASHTO) *LFRD Bridge Design Specifications*, were applied to the bridge deck to maximize shear, flexure, and torsion in the skewed bridge. Live load distribution between the three girders was approximately equal and the assumption of strain compatibility between the bridge deck, FRP shell, and steel strand was confirmed. Stresses in bottom flange FRP strands and the top of deck concrete were less than 30% of material limits under service level live loads. The concrete arch fell below the composite neutral axis, placing it in tension along the span.

After the live load system tests, a more detailed investigation was performed in Phase 4 to explore transverse deck behavior. Transverse flexural demands were approximately 20% of the design capacity and standard truss bars, as specified by the Virginia Department of Transportation, are not necessary because of the small clear span of the slab between beams. In Phase 5, the bridge system was saw-cut longitudinally to separate it into three individual HCB composite beams. Two beams were load tested to failure at the Structures Laboratory at Virginia Tech. For one of the two beams tested at Virginia Tech, 14 out of a total 22 strands were cut at mid-span to simulate strand deterioration and for comparison the other beam remained undamaged prior to testing. The observed beam failure modes were mid-span concrete crushing for the undamaged beam and mid-span strand-FRP bond failure for the damaged beam. In support of Phase 5, a three-dimensional (3D) finite element model was developed to explore flexural and shear force distributions along the span, which led to a shear design procedure in which shear force is distributed based on the relative moments of inertia of the FRP shell and arch. Shear resistance is provided by the FRP shell webs and the concrete arch and fin.

FINAL REPORT

FULL-SCALE LABORATORY EVALUATION OF HYBRID COMPOSITE BEAMS FOR IMPLEMENTATION IN A VIRGINIA BRIDGE

Cristopher D. Moen, Ph.D., P.E.
CEO and President
NBM Technologies, Inc.

Carin L. Roberts-Wollmann, Ph.D., P.E.
Professor
The Charles E. Via, Jr. Department of Civil and Environmental Engineering
Virginia Polytechnic Institute and State University

Thomas E. Cousins, Ph.D., P.E.
Professor
Glenn Department of Civil Engineering
Clemson University

VTRC Project Manager
Bernard L. Kassner, Ph.D., P.E., Virginia Transportation Research Council

DISCLAIMER

The project that is the subject of this report was done under contract for the Virginia Department of Transportation, Virginia Transportation Research Council. The contents of this report reflect the views of the authors, who are responsible for the facts and the accuracy of the data presented herein. The contents do not necessarily reflect the official views or policies of the Virginia Department of Transportation, the Commonwealth Transportation Board, or the Federal Highway Administration. This report does not constitute a standard, specification, or regulation. Any inclusion of manufacturer names, trade names, or trademarks is for identification purposes only and is not to be considered an endorsement.

Each contract report is peer reviewed and accepted for publication by staff of the Virginia Transportation Research Council with expertise in related technical areas. Final editing and proofreading of the report are performed by the contractor.

ABSTRACT

This research project studied a steel-reinforced concrete and fiber-reinforced polymer (FRP) structural element called the Hybrid-Composite Beam (HCB). The beam was used in a skewed simple span superstructure replacement project over the Tides Mill Stream in Colonial Beach, Virginia. For typical HCB construction, each beam is transported to site as a lightweight FRP beam shell. Self-consolidating concrete is pumped into the shell interior arch form, and when the concrete hardens, it stiffens and strengthens the beam so that it can act as falsework to carry the weight of a cast-in-place concrete bridge deck. Unstressed prestressing strands are embedded in the FRP shell bottom flange during the resin placement, and these strands equilibrate thrust in the arch and stiffen the beam to meet service deflection criteria. After the deck is placed, the HCB system performs as a longitudinal flexural member, with the bridge deck resisting compression and prestressing strands and the FRP bottom flange resisting tension.

The primary research goal was to document the HCB as a structural component and as a bridge system, with the outcome being validation of key assumptions that can be applied to future designs such as, for example, strain compatibility between the FRP shell and steel strands. The research was conducted in five phases. In Phase 1, the HCB flexural rigidity and through-depth strain distributions were quantified considering just the FRP shell with unstressed strands. These tests confirmed flexural rigidity estimated by hand calculations and strain compatibility under uniform loads. Phase 2 evaluated flexural behavior of the HCB FRP shell and poured concrete arch. Phase 3 testing was performed after three HCBs were made integral with cast-in-place concrete end diaphragms and a reinforced concrete bridge deck. Point loads, to simulate an HL-93 design truck as specified in American Association of State Highway and Transportation Officials (AASHTO) *LFRD Bridge Design Specifications*, were applied to the bridge deck to maximize shear, flexure, and torsion in the skewed bridge. Live load distribution between the three girders was approximately equal and the assumption of strain compatibility between the bridge deck, FRP shell, and steel strand was confirmed. Stresses in bottom flange FRP strands and the top of deck concrete were less than 30% of material limits under service level live loads. The concrete arch fell below the composite neutral axis, placing it in tension along the span.

After the live load system tests, a more detailed investigation was performed in Phase 4 to explore transverse deck behavior. Transverse flexural demands were approximately 20% of the design capacity and standard truss bars, as specified by the Virginia Department of Transportation, are not necessary because of the small clear span of the slab between beams. In Phase 5, the bridge system was saw-cut longitudinally to separate it into three individual HCB composite beams. Two beams were load tested to failure at the Structures Laboratory at Virginia Tech. For one of the two beams tested at Virginia Tech, 14 out of a total 22 strands were cut at mid-span to simulate strand deterioration and for comparison the other beam remained undamaged prior to testing. The observed beam failure modes were mid-span concrete crushing for the undamaged beam and mid-span strand-FRP bond failure for the damaged beam. In support of Phase 5, a three-dimensional (3D) finite element model was developed to explore flexural and shear force distributions along the span, which led to a shear design procedure in which shear force is distributed based on the relative moments of inertia of the FRP shell and arch. Shear resistance is provided by the FRP shell webs and the concrete arch and fin.

FINAL REPORT

FULL-SCALE LABORATORY EVALUATION OF HYBRID COMPOSITE BEAMS FOR IMPLEMENTATION IN A VIRGINIA BRIDGE

Cristopher D. Moen, Ph.D., P.E.
CEO and President
NBM Technologies, Inc.

Carin L. Roberts-Wollmann, Ph.D., P.E.
Professor
The Charles E. Via, Jr. Department of Civil and Environmental Engineering
Virginia Polytechnic Institute and State University

Thomas E. Cousins, Ph.D., P.E.
Professor
Glenn Department of Civil Engineering
Clemson University

INTRODUCTION

In 2013, the Virginia Department of Transportation (VDOT) replaced the steel stringer superstructure over the Tides Mill Stream in Colonial Beach, Virginia, with a new type of hybrid composite beam (HCB) system, as shown in Figure 1. Each HCB is made up of a fiber-reinforced polymer (FRP) shell that contains a concrete arch and unstressed prestressing strands that equilibrate the arch thrust and serve as flexural reinforcement (along with the FRP bottom flange). The newly constructed bridge has a simple span that is 48 ft-4 in in length with 8 HCBs spaced at 4 ft on center and arranged at a 45-degree skew (Figure 2).


| (a) | (b) |

Figure 1. Bridge Over Tides Mill Stream on State Route 205 in Colonial Beach, Virginia: (a) Elevation View Looking North and (b) Elevation View Looking East

(a)

(b)

Figure 2. Tides Mill Stream (a) Plan and (b) Full-Width Section Drawings

2

This bridge type was first tested for short-span rail bridges as a rapid construction alternative to heavy steel and concrete girders (Hillman, 2003; Hillman, 2008). The HCB was extended to short-span highway bridges with research through the Advanced Structures and Composites Center at the University of Maine (Snape and Lindyberg, 2009). The study concluded that the HCB can be analyzed and designed with a linear-elastic strain compatibility approach and that no stiffness degradation was observed after 2 million flexural fatigue cycles to simulate truck traffic. The FRP shell was evaluated under accelerated weathering treatments without observed deterioration and, based on these positive results, the Maine Department of Transportation proceeded with the replacement of the 8-span, 540-ft-long Knickerbocker Bridge in Boothbay, Maine, using the HCB system.

A typical HCB construction sequence is as follows. The FRP shells are transported to site and lifted into place with a light derrick crane onto elastomeric bearings. Self-consolidating concrete is pumped into arch forms inside each FRP shell. When the concrete hardens, the arch-stiffened FRP shells serve as falsework for a cast-in-place concrete bridge deck. The bridge deck is made composite with the HCBs using inclined steel stirrups that are embedded in each concrete arch, as shown in Figure 3.

The HCB system was selected for the Virginia trial implementation because it was predicted to decrease construction time over traditional methods. The beams are lighter than those of typical steel construction, which would permit the use of the existing abutments. Also, the bridge passes over brackish water and it is hypothesized that the FRP shell would provide maintenance-free service life consistent with a precast concrete voided slab bridge. The research program design, details, and results are summarized in the following sections.
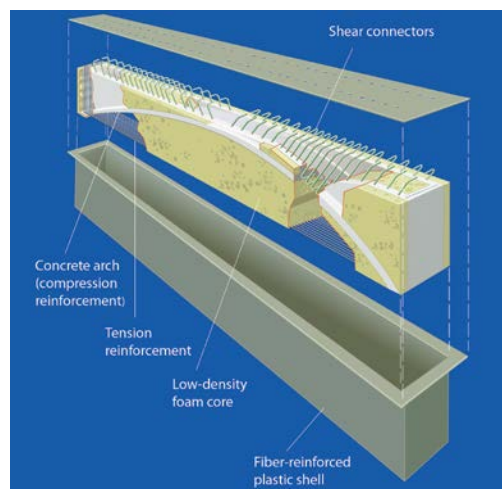
Figure 3. HCB Isometric Showing the FRP Shell, Foam Core Supporting the Internal Arch Form, and Shear Stirrups That Develop Composite Action With a Cast-in-Place Concrete Bridge Deck

PURPOSE AND SCOPE

This report summarizes the HCB research program conducted at Virginia Tech in support of the Tides Mill Stream HCB implementation. The primary research study goals were: (1) study HCB service and ultimate limit states behavior with experiments; (2) validate HCB design

procedures proposed by the patent holder, the H.C. Bridge Company; and (3) gain experience with HCB construction.

The research scope was defined as a multi-phase experimental program. Three HCB beam specimens were fabricated by Harbor Technologies in Brunswick, Maine, and shipped to Virginia Tech in October 2011. Phase 1 tests focused on flexural response of the HCB FRP shell; Phase 2 evaluated flexural behavior of the HCB FRP shell and poured concrete arch; Phase 3 involved simulated HL-93 live load system tests to study live load distribution factors and the skew effect in a three HCB bridge with a cast-in-place bridge deck; Phase 4 involved additional simulated HL-93 live load tests to further assess transverse load effects on the deck of the three-beam bridge; and in Phase 5 the bridge was saw-cut longitudinally into three individual beams with composite concrete deck sections, two of which were load tested to collapse with one of the two having imposed prestressing strand damage at mid-span. The third beam was sent to the Army Corps of Engineers in Champaign, Illinois, for long-term corrosion tests. Computational models were developed in the commercial finite element program ABAQUS (Simulia, 2014) to supplement the Phase 5 testing. The model observations lead to a shear strength capacity prediction procedure that is presented later in this report.
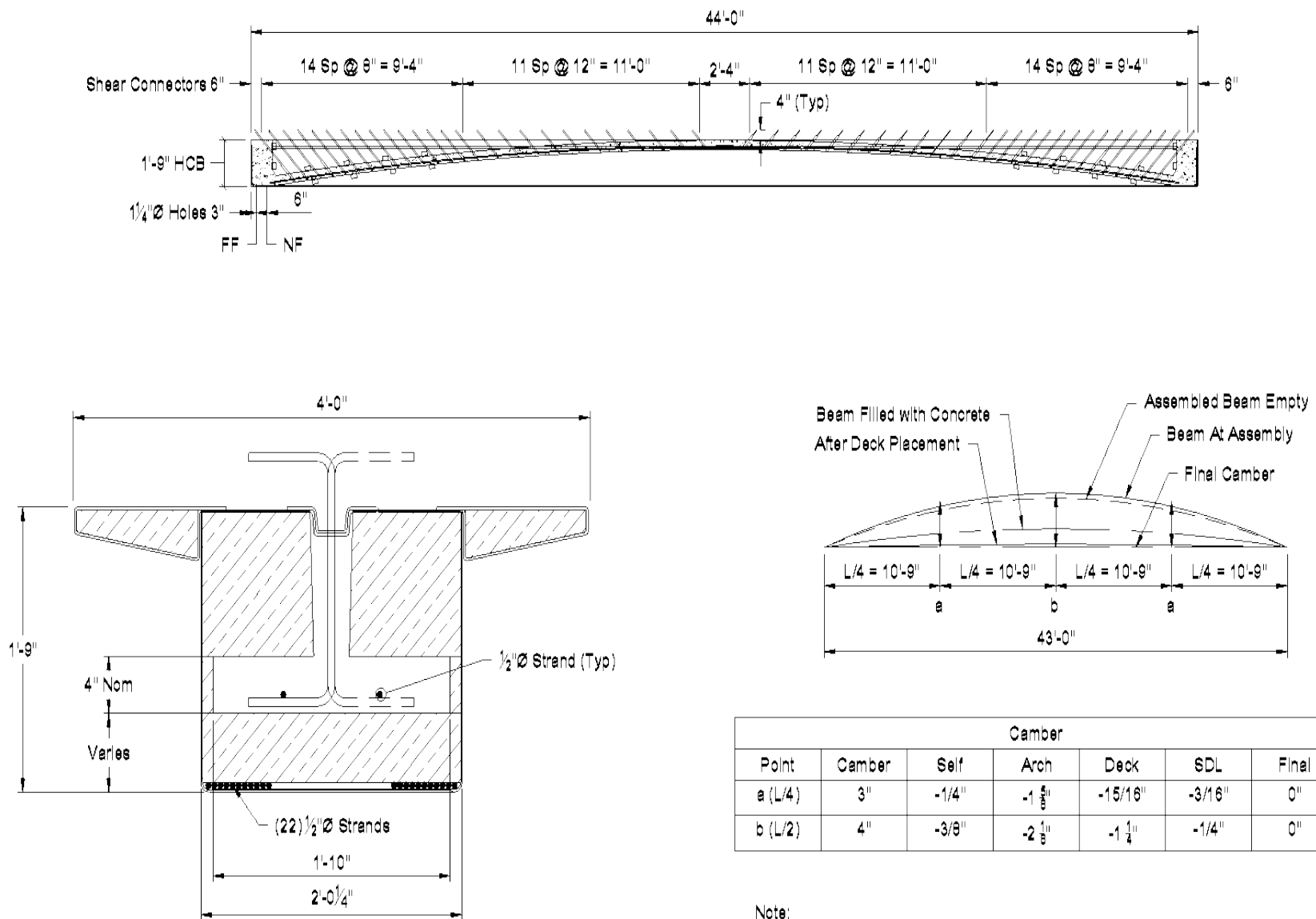
METHODS

The HCB research program consisted of experimental programs (Phases 1 through 5 described previously) designed to develop and validate HCB design procedures. The methods employed in these phases are introduced here. Each of the three HCB specimens studied (labeled HCB1, HCB2, and HCB3) was 44 ft long with cross-section and arch details as documented in Figure 4 and a plan view of the entire system in Figure 5. Full experimental details for each phase are documented in supporting documents generated by graduate students at Virginia Tech (Ashan, 2012; Bajzek, 2012; Mascaro and Moen, 2012; Van Nosdall, 2013).

Phase 1: FRP Shell Under Uniform Load Tests

Uniform load flexural tests were performed on just the HCB FRP shell as shown in Figure 6, after the beam lid was glued to the FRP shell (Figure 7a), and before the arch concrete was placed, to experimentally determine flexural rigidity. These measurements were used to confirm the assumed quasi-isotropic FRP constitutive laws used throughout the design calculations and in the computational model efforts. The flexural rigidity measurements also provided a measure of how much the stay-in-place wing forms contributed to flexural stiffness, and they confirmed that a transformed area approach for the prestressing strands embedded in the bottom of the shell could be used to calculate the moment of inertia of the beam.

This Phase 1 testing consisted of loading individual FRP shells with steel angles to simulate a uniform load. A total of 85 angles were placed on each of specimens HCB1, HCB2, and HCB3 to achieve an approximate distributed load of 50 lb/ft. The beam support boundary conditions were pinned-roller (43 ft from center to center of bearings) and wire potentiometers were placed at each quarter point and mid-span to measure vertical deflection.

Elevation drawing labels:
- 44'-0"
- Shear Connectors 6"
- 14 Sp @ 8" = 9'-4"
- 11 Sp @ 12" = 11'-0"
- 2'-4"
- 11 Sp @ 12" = 11'-0"
- 14 Sp @ 8" = 9'-4"
- 6"
- 4" (Typ)
- 1'-9" HCB
- 1¼"Ø Holes 3"
- 6"
- FF
- NF

Section drawing labels:
- 4'-0"
- 1'-9"
- 4" Nom
- Varies
- ½"Ø Strand (Typ)
- (22) ½"Ø Strands
- 1'-10"
- 2'-0¼"

Camber diagram labels:
- Beam Filled with Concrete After Deck Placement
- Assembled Beam Empty
- Beam At Assembly
- Final Camber
- L/4 = 10'-9"
- L/4 = 10'-9"
- L/4 = 10'-9"
- L/4 = 10'-9"
- a
- b
- a
- 43'-0"

Camber						
Point	Camber	Self	Arch	Deck	SDL	Final
e (L/4)	3"	-1/4"	-1 5/8"	-15/16"	-3/16"	0"
b (L/2)	4"	-3/8"	-2 1/8"	-1 1/4"	-1/4"	0"

Note:
   Camber in mold for bottom section is 2 ¼" (See Dwg HCB-Beam-2). Block bottom section up to 4" camber at midspan prior to beam assembly.

Figure 4. Elevation and Section Drawings for HCBs Tested at Virginia Tech

5
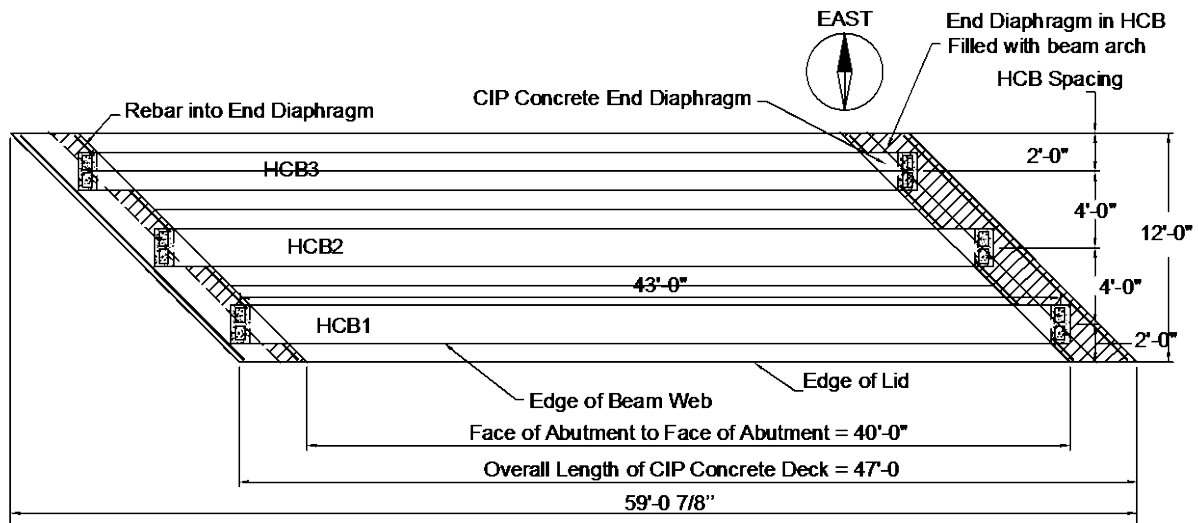
Figure 5. Plan Drawing for HCB System Tested at Virginia Tech
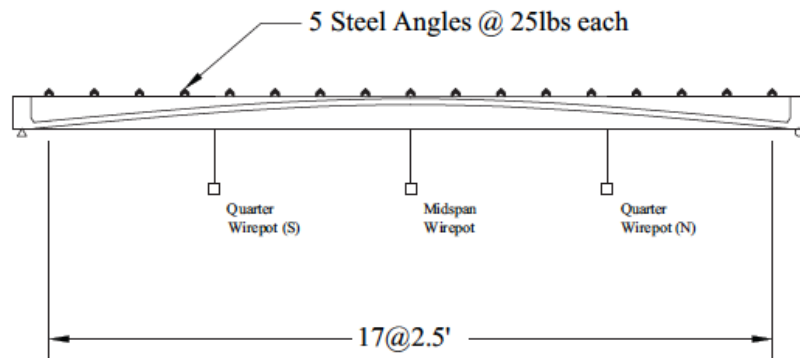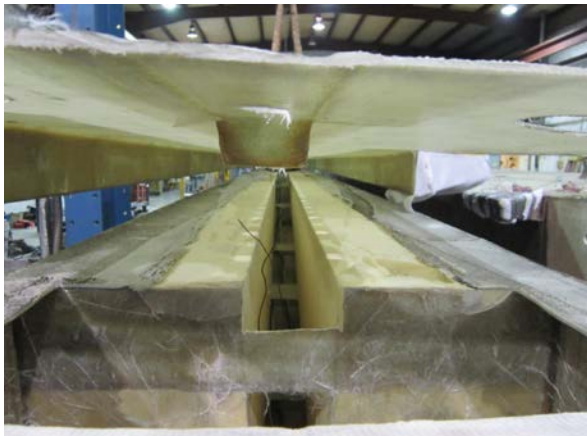

Figure 6. Phase 1 FRP Shell Loading and Instrumentation

(a)

(b)

Figure 7. (a) HCB FRP Lid Is Lifted Into Place Before Gluing and (b) Self-Consolidating Concrete Is Pumped Into the Internal HCB Arch Form Through a Hole in the Lid

Phase 2: FRP Shell and Concrete Arch Under Four-Point Bending

After the Phase 1 tests were concluded, shear reinforcement was placed in each HCB specimen. Self-consolidating concrete was pumped into the arch cavities (Figure 7b) through holes in the top flange lid. The concrete flowed down the arch until it filled the prestressing strand anchor blocks at the beam ends. The selected self-consolidating concrete mix design, with a water to cement ratio of 0.35, is summarized in Table 1.

Table 1. Self-Consolidating Arch Concrete Mix Design

Ingredient	Quantity
Type II cement	652 lb/yd^3
Silica fume	53 lb/yd^3
#8 ACCO 57 crushed limestone large aggregate	1750 lb/yd^3
Wythe natural sand fine aggregate	1303 lb/yd^3
Water	29.5 lb/yd^3
Air by volume	5.5% by volume
Air entraining admixture	42 mL/yd^3
Water reducing and retarding admixture	730 mL/yd^3
High range water reducing admixture	834 mL/yd^3

Three-point and four-point bending tests were conducted on the HCB in its state as a stay-in-place form for a concrete deck where the FRP and arch are working together as a tied arch. Applied loads were kept below 50% of the cast-in-place concrete deck weight to limit stresses in the beam. The goal was to study load-deformation response and flexural rigidity of the FRP and arch together to determine if a transformed area approach is appropriate in this state for calculating deflections. Strain gages in the concrete arch and FRP shell shown in Figures 8 and 9 allowed for the study of the force distribution in the arch and the FRP shell, both important for the design of the HCB during the deck pouring phase (Van Nosdall et al., 2013).
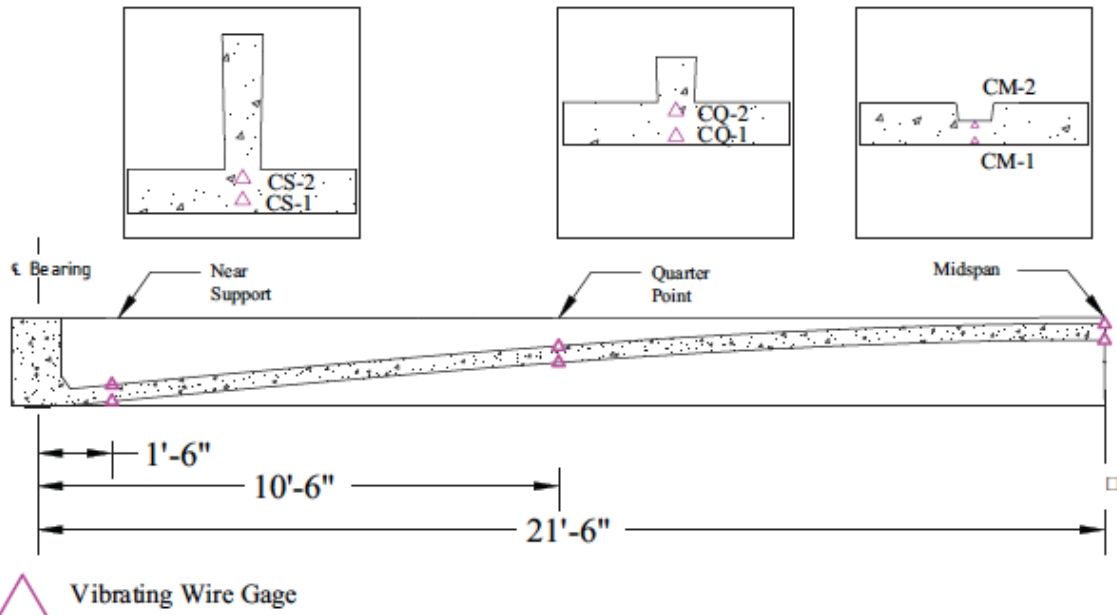
Figure 8. Vibrating Wire Strain Gage Locations in the Concrete Arch (Typical for HCB1, HCB2, and HCB3)
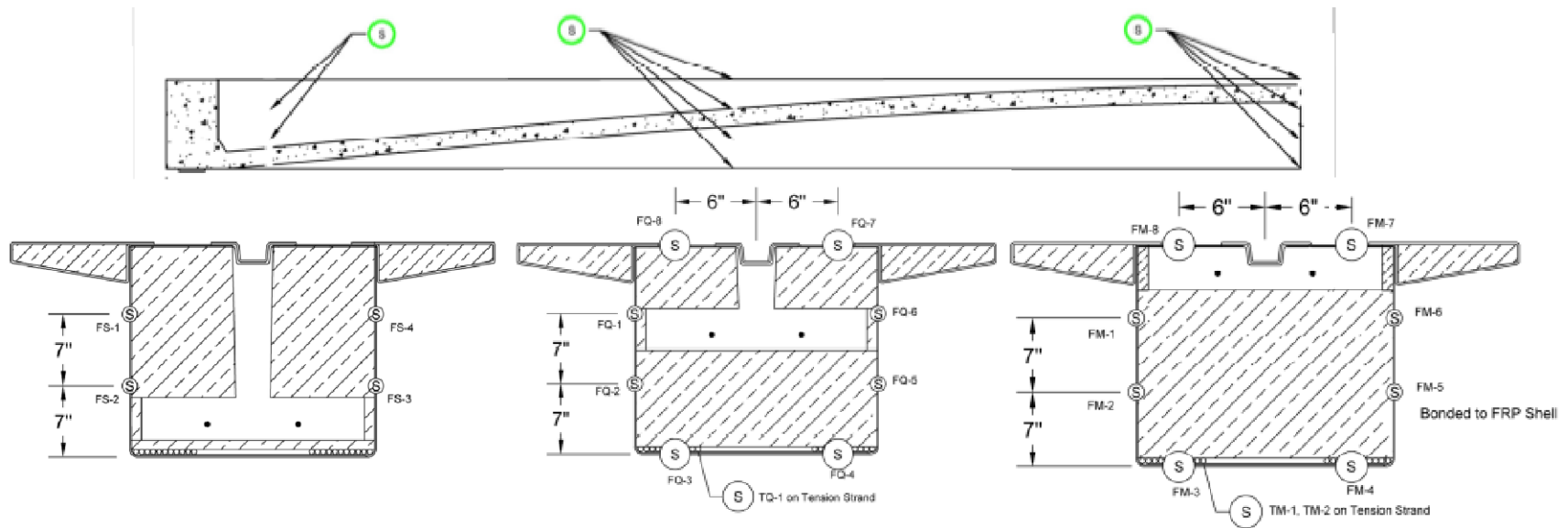
Figure 9. Foil Strain Gage Locations Around FRP Shell (Typical for HCB1, HCB2, and HCB3)

Phase 2 testing commenced 45 days after the arch concrete was poured. For HCB1, HCB2, and HCB3, vertical deflections and quarter-span and mid-span strains were measured in the FRP shell, steel strand, and arch concrete under a 15-kip point load at mid-span and two 12.5-kip point loads at quarter points. The beams rested on the same pin and roller boundary conditions used in Phase 1. Concrete testing for the arch concrete was performed using established American Society for Testing and Materials (ASTM) procedures, including ASTM C39-05, Standard Test Method for Compressive Strength of Cylindrical Concrete Specimens (2014), ASTM C496-04, Standard Test Method for Splitting Tensile Strength of Cylindrical Concrete Specimens (2004), and ASTM C469-02, Standard Test Method for Static Modulus of Elasticity and Poisson's Ratio of Concrete in Compression (2014).

Phase 3: Superstructure System Tests Under HL-93 Loading

This phase focused on service live load tests of a skewed three-beam HCB system built in the Structures Lab at Virginia Tech; see Figure 5 for a plan view. The applied loads simulated those of an HL-93 design truck in accordance with the American Association of State Highway and Transportation Officials (AASHTO) LFRD Bridge Design Specifications (2009). The bridge deck depth of 7.5 in and transverse reinforcing bar size and spacing (No. 5 bars at 7 in on center with alternating truss and straight bars) were selected based on the VDOT Manual of the Structure and Bridge Division (Volume V, Part 2, Chapter 10, Sheets 1–12) (VDOT 2011) for a 4-ft transverse beam spacing. The bridge deck and end diaphragms were placed with standard A4 VDOT concrete (VDOT, 2008); see Figure 10. Concrete testing was performed using established ASTM procedures, including ASTM C39-05 (2014) for compressive strength, ASTM C496-04 (2004) for splitting tensile strength, and ASTM C469-02 (2014) for elastic modulus.

Figure 10. HCB Bridge Deck (a) Rebar and Formwork; (b) Concrete Placement

Combinations of point loads were applied to simulate HL-93 axle loads as shown in Figure 11. The magnitude of each point load applied to the bridge was 21.3 kips, which is the weight of two rear axles of an HL-93 truck (64 kips) divided by four wheels and multiplying by a dynamic load factor of 1.33. The wheel patches were spaced at 14 ft longitudinally and 6 ft transversely. Wire potentiometers were employed to measure beam deflections and quantify load distribution as shown in Figure 12.

In Tests 1 and 2, the wheel loads were centered longitudinally on the bridge and placed transversely such that the west wheel line was on the HCB1 centerline. For Tests 3 and 4, the
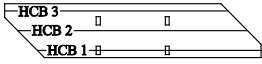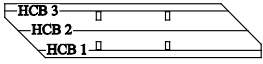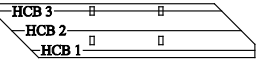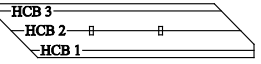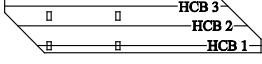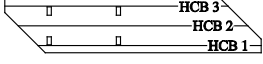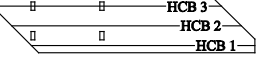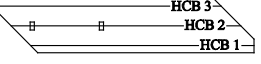
Figure 11. Phase 3 Superstructure System Tests With AASHTO HL-93 Load Cases. Each Rectangle Denotes a Load Footprint.

Figure 12. Wire Potentiometers Arranged at HCB Quarter Points and Mid-span

wheel loads were moved east 1 ft so that the two wheel lines straddled HCB2. Tests 5 and 6 placed the east wheel line directly over the centerli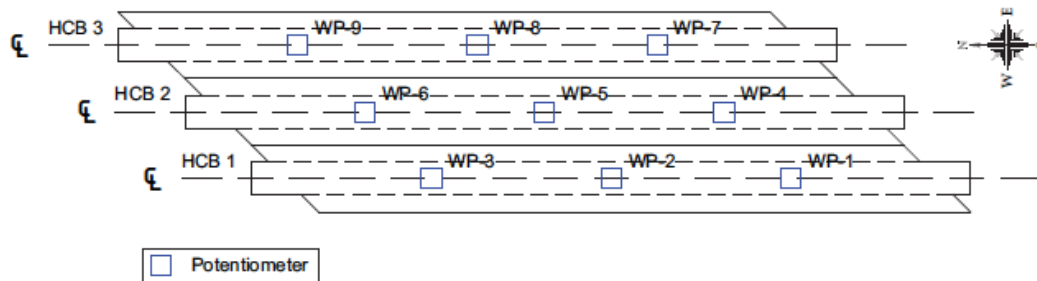ne of HCB3. For Tests 7 through 12, longitudinal locations were adjusted to maximize shear in the beams by locating the rear truck axle adjacent to the support, with the wheel lines in the same transverse locations as Tests 1 through 6, respectively.

After tests to simulate axle loads were concluded, Tests 13 through 17 were conducted to represent one wheel line (two wheel patch loadings placed 14 ft apart longitudinally) that were placed directly over the centerline of HCB2. The wheel patch load was 21.3 kips. The maximum shear tests (Tests 13 and 14) were performed so that the north patch of the wheel line was approximately 2 ft from the centerline support. The maximum moment tests (Tests 15 and 16) were conducted with the wheel line longitudinally centered over the mid-span of HCB2 and transversely centered on HCB2. Detailed drawings and dimensions for each live load configuration are provided in Ahsan (2013), Appendix D.

Phase 4: Bridge Deck Tests Under HL-93 Loads

This phase was designed to characterize HCB transverse bridge deck behavior of the three-beam system previously introduced in Phase 3. As shown in Figure 13, there were a total of nine tests where wheel patch loads with two different magnitudes (Tests 1-7 with service loads, Tests 8 and 9 with ultimate loads) were applied to test transverse deck bending with adhesive strain gauges attached to the reinforcing steel and vibrating wire strain gauges embedded in the concrete (see Figure 14). A shell finite element model was also developed and validated to study 3D deck bending and skew effects (Bajzek, 2013).
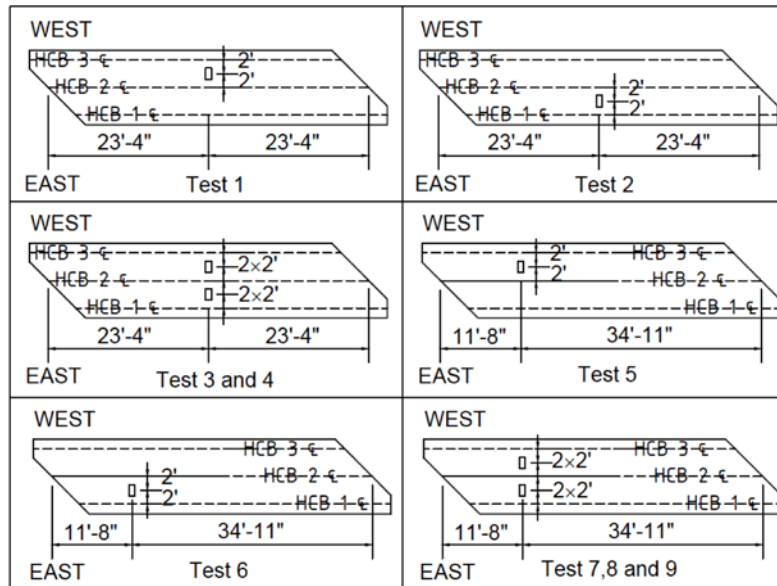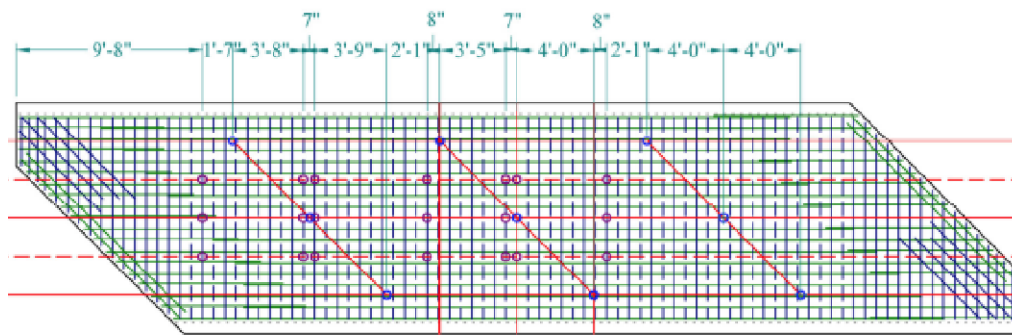
10

Figure 13. Phase 4 Bridge Deck Tests With AASHTO HL-93 Load Cases

Figure 14. Instrumentation Map and Nomenclature for Phase 4 Bridge Deck Tests

11

Phase 5: Ultimate Strength Tests

After the Phase 4 bridge deck tests, the three-beam system was longitudinally saw-cut into individual beams, resulting in three HCB specimens, each with a composite concrete bridge deck. Two of the specimens were tested to failure in four-point bending with the goal of comparing the tested strengths to calculated predictions. HCB1 was tested as an undamaged simple span (see Figure 15a). Damage was induced in HCB2, with 14 of the 22 prestressing strands cut at mid-span as shown in Figure 15b and Figure 15c. Strains and load-deformation response of the concrete, FRP, and strands were recorded for both tests.
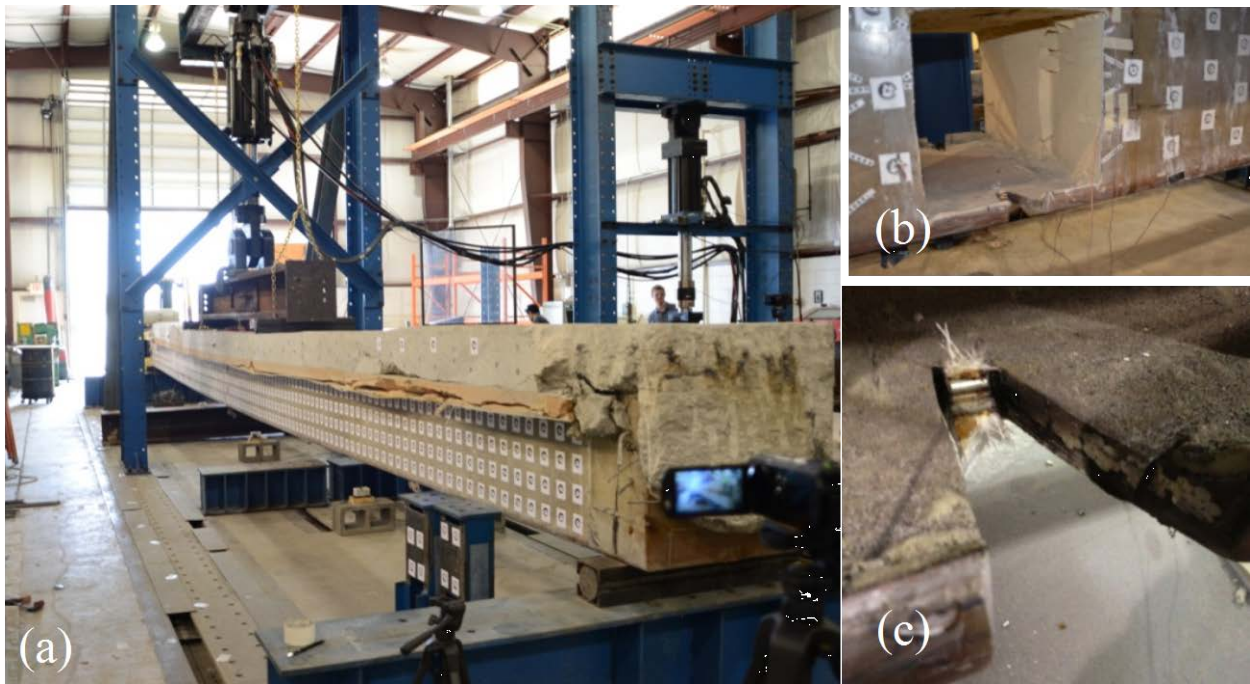
Figure 15. Phase 5 Four-Point Bending Tests: (a) Undamaged Beam HCB1; (b, c) HCB2 With Prestressing Strands Cut at Mid-span

A 3D finite-element model was developed in ABAQUS (Figure 16) to allow study of load distribution within the HCB during the flexural tests and to explore how the beam carries shear to the supports. The concrete slab, end diaphragms, arch, and interior foam were modeled with meshed eight-node (C3D8R) solid elements. The concrete constitutive law is elastic–perfectly plastic with an elastic modulus of 3,640 ksi and compressive strength of 4,000 psi. The FRP shell was modeled with four-node (S4R) shell elements, and the prestressing strands with 3D (T3D2) truss elements. The FRP anisotropic behavior was simulated by assigning an elastic modulus of 3,100 ksi along the beam and 2,300 ksi vertically (see Table 2). The FRP shell was constructed of quad-weave glass fibers infused in a vinyl ester resin, where the quad-weave consisted of four fiber layers oriented in four (0, 45, -45, and 90 degree) directions.
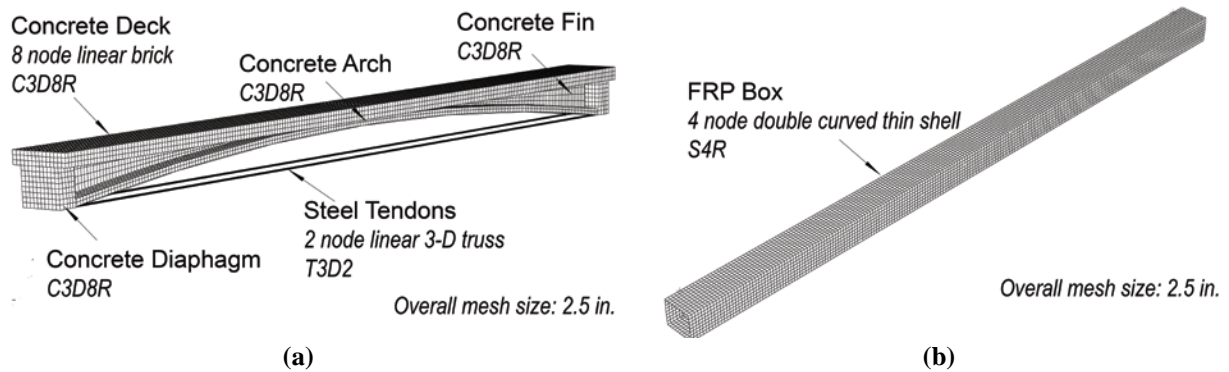
Figure 16. HCB Finite Element Models: (a) Concrete Arch and Composite Bridge Deck and (b) FRP Shell

Table 2. Material Properties Provided by Manufacturer for the HCB Fiber-Reinforced Polymer Shell

Property	Value
Resin Unit Weight	0.54 b/ft²
Fiber Unit Weight	0.93 lb/ft²
Laminate Unit Weight	1.47 lb/ft²
Volume Fraction	45% by Volume
0° Modulus, E_x	3,100 ksi
90° Modulus, E_y	2,300 ksi
Shear Modulus	1,010 ksi
0° Tensile Ultimate Stress	27.8 ksi
90° Tensile Ultimate Stress	20.6 ksi
Shear Ultimate Stress	19.1 ksi
0° Compressive Ultimate Stress	27.8 ksi
90° Compressive Ultimate Stress	20.6 ksi

RESULTS AND DISCUSSION

Measured Concrete Material Properties

Arch, bridge deck, and end diaphragm concrete properties in the hardened state were carefully documented. The self-consolidating concrete design compressive strength used for the arches in the HC Bridge Company calculations was 6,000 psi and, as shown in Table 3, the average measured strength is consistent, showing some minimal variations after 28 days. The average A4 concrete compressive strength for the end diaphragms and bridge deck exceeded the minimum 4,000 psi requirement at 28 days except for the bridge deck Batch 2, which was 3,500 psi (see Table 4 and Table 5, respectively). Batch 2 compressive strength was above 4,000 psi at the time of structural testing however.

Table 3. Arch Concrete Properties in the Hardened State

Day	Compressive Strength (psi)	Splitting Tensile Strength (psi)	Modulus of Elasticity (ksi)
7	5,120 (3)	-	-
14	5,360 (3)	-	-
28	6,190 (3)	635 (2)	4,480 (2)
45	5,680 (3)	605 (2)	3,900 (2)
206	5,910 (2)	520 (2)	3,820 (2)

Values in Parentheses Indicate Number of Tests

Table 4. Diaphragm Concrete Properties in the Hardened State

Day	Compressive Strength (psi)	Splitting Tensile Strength (psi)	Modulus of Elasticity (ksi)
7	4,180 (2)	-	4,480 (2)
14	4,360 (3)	-	4,680 (2)
28	4,870 (2)	545 (2)	5,250 (2)
61	5,730 (2)	460 (2)	4,390 (2)

Values in Parentheses Indicate Number of Tests

Table 5. Bridge Deck Concrete Properties in the Hardened State

Day	Batch	Compressive Strength (psi)	Splitting Tensile Strength (psi)	Modulus of Elasticity (ksi)
7	Batch 1	3,460 (2)	-	3,890 (2)
	Batch 2	2,690 (2)	-	3,420 (2)
14	Batch 1	4,400 (2)	-	4,650 (2)
	Batch 2	3,280 (2)	-	4,000 (2)
21	Batch 1	4,580 (2)	-	4,620 (2)
	Batch 2	3,440 (2)	-	4,230 (2)
28	Batch 1	4,480 (2)	525 (2)	4,950 (2)
	Batch 2	3,500 (2)	440 (3)	4,390 (2)
40	Batch 1	4,820 (2)	505 (2)	4,700 (2)
	Batch 2	4,060 (2)	430 (2)	6,880 (2)

Values in Parentheses Indicate Number of Tests

Phase 1: FRP Shell Uniform Load Tests

Measured and predicted HCB shell vertical deflections for a 50 lb/ft uniform load (and simple span of 43 ft) are summarized in Table 6. These tests were performed to confirm flexural rigidity assumptions made in the design calculations (E=3,100 ksi, I=3,010 in^4). The HCB2 and HCB3 beams were loaded and unloaded twice and this is why there are two sets of results per beam in Table 6. The predicted deflections are on average 25% higher than the measured. It is hypothesized that the beam wings, which were not included in the deflection calculation, contributed additional stiffness. The actual FRP elastic modulus could also be higher than what was assumed.

Table 6. Phase 1 FRP Shell Mid-Span Deflections Under Uniform Load: Measured Versus Predicted

HCB	Measured Deflection (in)	Predicted Deflection (in)	Measured/ Predicted
3	0.33	0.41	0.80
3	0.33	0.41	0.80
2	0.29	0.41	0.71
2	0.29	0.41	0.71
1	0.33	0.41	0.80

The HCB1 beam was instrumented with strain gauges on the FRP shell and on two of the steel prestressing strands as denoted in Figure 8 and the insets of Figure 17. This strain gauge set was placed at beam mid-span. For the uniform load of 50 lb/ft, the strain profile through the FRP shell depth is nonlinear, with a neutral axis located approximately 7 in from the bottom fiber, compared to a calculated neutral axis location of 5 in. The result provides more supporting evidence that the beam wings contribute to the beam's flexural rigidity. It is hypothesized that the strain profile nonlinearity is caused by shear deformation that violates the fundamental Euler-Bernoulli assumption of plane sections. This nonlinearity is common in FRP members because the epoxy polymer in the FRP shell has a shear modulus that is 10 times less than that of concrete. Strand and bottom flange FRP strain gauge readings are consistent (compare TM-1 and FM-3, TM-1 and FM-4 in Figure 17), which demonstrate that there is bond and strain compatibility provided by the epoxy infusion during manufacturing.
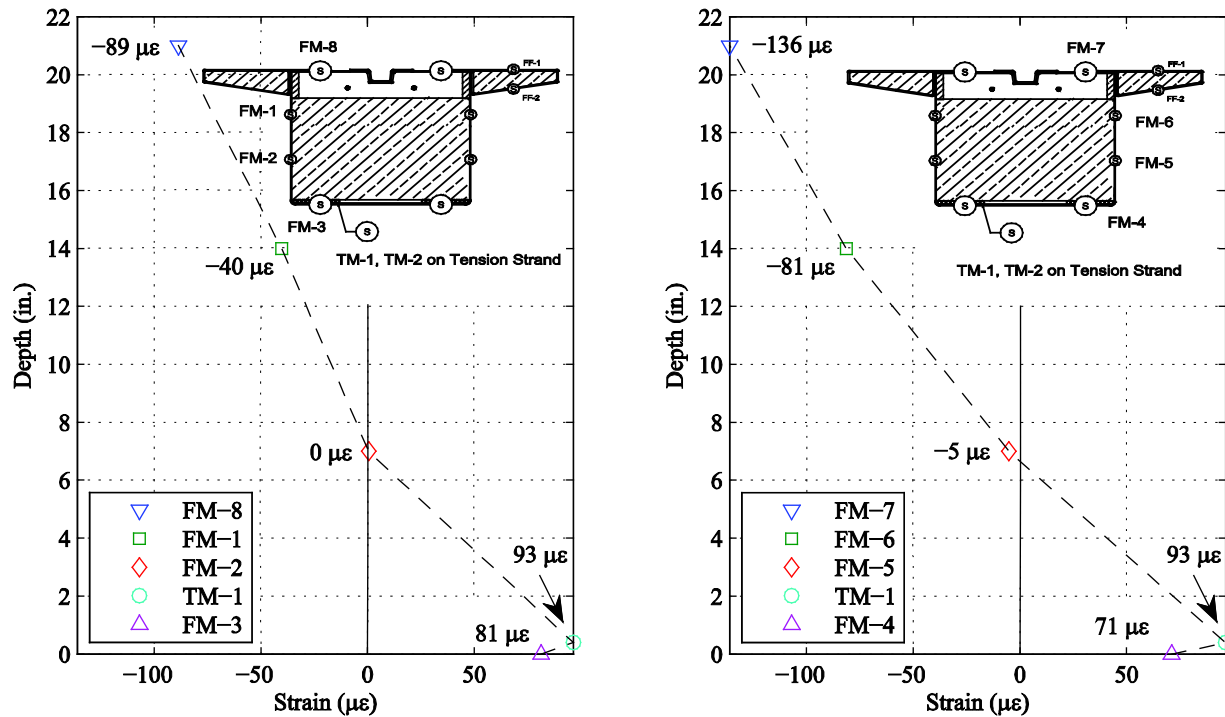
Figure 17. Phase 1 HCB1 FRP Shell Uniform Load Strain Profiles at Mid-span

15

Phase 2: FRP Shell and Concrete Arch Four-Point Bending Tests

The measured mid-span deflection values from the Phase 2 testing (poured arch and FRP shell) are presented in Table 7 for a single 15-kip point load at mid-span and in Table 8 for two 12.5-kip quarter-span loads. The load-deformation responses were linear throughout the tests. For both loading types, the measured deflections were approximately 25% less than the predicted values, as calculated with transformed section properties.

Table 7. Mid-Span Deflection for 15-kip Mid-Span Point Load

HCB	Measured Deflection (in)	Predicted Deflection (in)	Measured/ Predicted
1	1.56	2.11	0.74
2	1.59	2.11	0.75
3	1.57	2.11	0.74

Table 8. Mid-span Deflection for 12.5-kip Quarter-Point Loads

HCB	Measured Deflection (in)	Predicted Deflection (in)	Measured/ Predicted
1	1.77	2.29	0.77
2	1.78	2.29	0.78
3	1.82	2.29	0.79

Representative strain profiles constructed using strain gages on the FRP shell, strain gages on the prestressing strand, and concrete arch vibrating wire gages are shown in Figure 18a for a single mid-span load (15 kips) and in Figure 18b for a quarter-point loading (two 12.5-kip point loads).   The strain trends are consistent with the transformed section analysis (dashed lines) in the compression region. The measured neutral axis is approximately 10% lower than predicted in Figure 18 and approximately 15% less strain was measured than predicted at the tensile outer fiber. It is hypothesized that the lower neutral axis and smaller measured tensile strains in both the prestressing strand and FRP shell result from the hardened epoxy that is not accounted for in the section property calculations.

Phase 3: Superstructure System Tests Under HL-93 Load

Phase 3 tests considered AASHTO HL-93 truck load at positions configured to produce upper bound moment, shear, and torsion in the three-beam system composite with a reinforced concrete bridge deck.   For each of the truck positions summarized in Figure 11, strains were recorded in the FRP shell, prestressing strands, and concrete arch.   Beam deflections were also measured to obtain live load distribution factors.

A typical strain profile is presented in Figure 19 for loading ST3 (wheel patches centered transversely on the bridge deck at mid-span longitudinally to develop maximum moment in beam HCB2).   The profile, taken at mid-span, has a linear trend with a neutral axis around 20 in from the tensile bottom fiber. This means the concrete arch is in tension (see red stars and readings of 98 and 114 microstrain in Figure 19) which was consistently observed throughout all the Phase 3 tests.

16
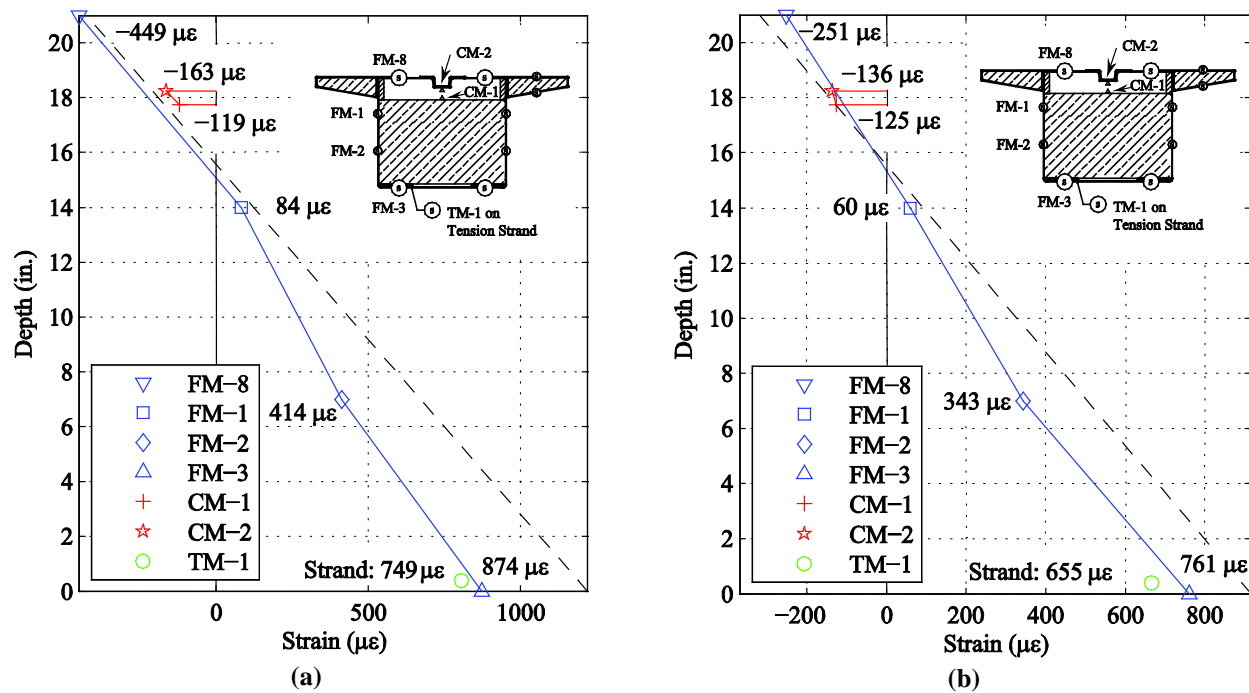
Figure 18. Mid-Span Strain Profiles for (a) HCB1 Loaded in Three-Point Bending (15-Kip Point Load at Mid-Span) and (b) for HCB1 Loaded in Four-Point Bending (Two 12.5-Kip Loads)
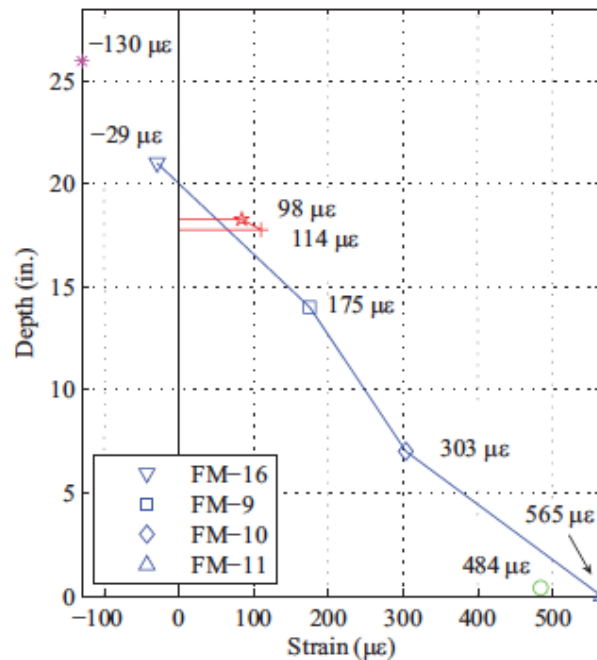
Figure 19. HCB2 Mid-Span Strain Profile for Loading ST3

From a service level design perspective, the stresses in all components were lower than material limits, except for the concrete arch.   FRP shell bottom fiber tensile strains varied from 275 to 620 microstrain, while the ultimate strain is reported by the manufacturer to be 8,970 microstrain.   Prestressing strand tensile strains ranged from 177 to 620 microstrain compared to an ultimate strain of 9,475 microstrain.   Concrete arch strains at the beam quarter points were all

17

measured to be in tension (250 to 990 microstrain) and larger than the concrete cracking tensile strain of 150 microstrain because the neutral axis is above the arch.

Maximum service live load mid-span deflections were approximately 0.80 in (developed for load cases ST1, ST2, and ST3) which corresponds to L/630, where L is span length in inches. Live load moment and shear distribution factors were derived from the deflection measurements, resulting in an even distribution of load on average (see Table 9 for moment distribution factors, shear trends are similar). The average live load moment distributions for the interior beams in the actual bridge at Tides Mill were in fact much lower (about 0.27), because the bridge is much wider and exhibits more plate behavior than the narrower (3-beam) specimen tested herein. However, the controlling distribution factor for the interior beams at the Tides Mill Bridge (0.35) was about the same as the mid-span distribution factors found in this study (Harris and Civitillo, (2017).

Table 9. Live Load Moment Distribution Factors Derived From Test-Measured Beam Deflections

Beam	Test	ST1	ST2	ST3	ST4	ST5	ST6	ST15	ST16	Average
HCB 1	North Quarter	0.40	0.40	0.36	0.35	0.32	0.35	0.34	0.35	0.36
	Mid-span	0.36	0.36	0.33	0.34	0.31	0.31	0.33	0.33	0.33
	South Quarter	0.30	0.29	0.27	0.27	0.25	0.25	0.31	0.26	0.28
	Average	0.35	0.35	0.32	0.32	0.29	0.31	0.33	0.31	0.32
HCB 2	North Quarter	0.31	0.31	0.31	0.36	0.36	0.30	0.38	0.34	0.33
	Mid-span	0.33	0.33	0.33	0.33	0.33	0.33	0.32	0.33	0.33
	South Quarter	0.35	0.35	0.34	0.36	0.34	0.34	0.32	0.34	0.34
	Average	0.33	0.33	0.33	0.35	0.34	0.32	0.34	0.34	0.33
HCB 3	North Quarter	0.29	0.30	0.32	0.29	0.32	0.35	0.28	0.31	0.31
	Mid-span	0.31	0.31	0.34	0.33	0.36	0.36	0.35	0.34	0.34
	South Quarter	0.36	0.36	0.39	0.37	0.41	0.41	0.37	0.39	0.38
	Average	0.32	0.32	0.35	0.33	0.36	0.38	0.33	0.35	0.34

Phase 4: Bridge Deck Testing Under HL-93 Load

Bridge deck behavior was evaluated for the three-HCB specimen by applying service and ultimate wheel load patch loadings (21.3 kips and 32.7 kips, respectively) at locations defined in Figure 13. The maximum vertical deck deflection for both service and ultimate loads occurred in Test Numbers 3 and 4, where two patch loads were applied at the longitudinal mid-span on either side of HCB2. The load-deformation responses for all service and ultimate load cases were linear with no cracking observed.

The maximum strains in the top and bottom mat transverse reinforcement for each test are summarized in Table 10. The maximum bottom mat tensile strains again occur in Test Numbers 3 and 4, which is consistent with the deflection trends in Table 11. The service strains in the steel are minimal relative to the reinforcing steel yield strain of 2,070 microstrain, and are approximately 30% of yield at ultimate loads for the Test Number 4 configuration. Compressive concrete strains in Table 12 are again highest for Test Number 3 (service) and Test Number 4 (strength) configurations; however, those strains are minimal when compared to the

Table 10. Summary of Maximum Transverse Measured Strain in Bridge Deck Top and Bottom Bars

Test Number – Load Type	Bottom Reinforcement Strain (με)	Top Reinforcement Strain (με)
1 - Service	217	17
2 - Service	305	72
3 - Service	347	92
4 - Strength	597	182
5 - Service	174	16
6 - Service	43	-23
7 - Service	201	41
8 - Strength	399	100
9 - Strength	402	9

Table 11. Summary of Maximum Measured Bridge Deck Deflections

Test Number – Load Type	Maximum Deflection (in)
1 - Service	-0.24
2 - Service	-0.27
3 - Service	-0.46
4 - Strength	-0.89
5 - Service	-0.22
6 - Service	-0.10
7 - Service	-0.34
8 - Strength	-0.61
9 - Strength	-0.58

Table 12. Summary of Largest Bridge Deck Compressive Longitudinal Measured Strain

| Test Number – Load Type	Strain (με)
1 - Service	-35
2 - Service	-91
3 - Service	-162
4 - Strength	-259
5 - Service	-70
6 - Service	-39
7 - Service	-135
8 - Strength	-225
9 - Strength	-224

concrete ultimate strain of 3,000 microstrain. The results demonstrate that the standard VDOT bridge deck design is conservatively designed for live load when applied to the HCB system.

## Phase 5: Ultimate Strength Tests

The ultimate strength flexural tests in four-point bending were performed to failure on two beams: one without damage (HCB1) and one with the FRP web removed and 14 prestressing strands cut at mid-span (HCB2). The flexural strengths of HCB1 and HCB 2 were 1,035 kip-ft with 8.4 in of mid-span deflection and 610 kip-ft with 5.0 in of mid-span deflection, respectively.

The HCB1 beam failed from concrete crushing at a loading point, as shown in Figure 20a, and the HCB2 failed by loss of bond between the prestressing strand and the FRP shell, as shown in Figure 20b. HCB1 also experienced FRP web delamination from the foam interior followed by diagonal buckling in the shear spans, as shown in Figure 21. This buckling did not initiate in the damaged beam HCB2 because high shear stresses in the FRP shell could not develop before failure. A vibration-based modal analysis of the damaged HCB2 demonstrated that the elastic flexural stiffness was minimally affected by cutting the steel strands, because most of the stiffness is derived from the composite concrete deck (Kernicky et al., 2015).

| (a) | (b) |
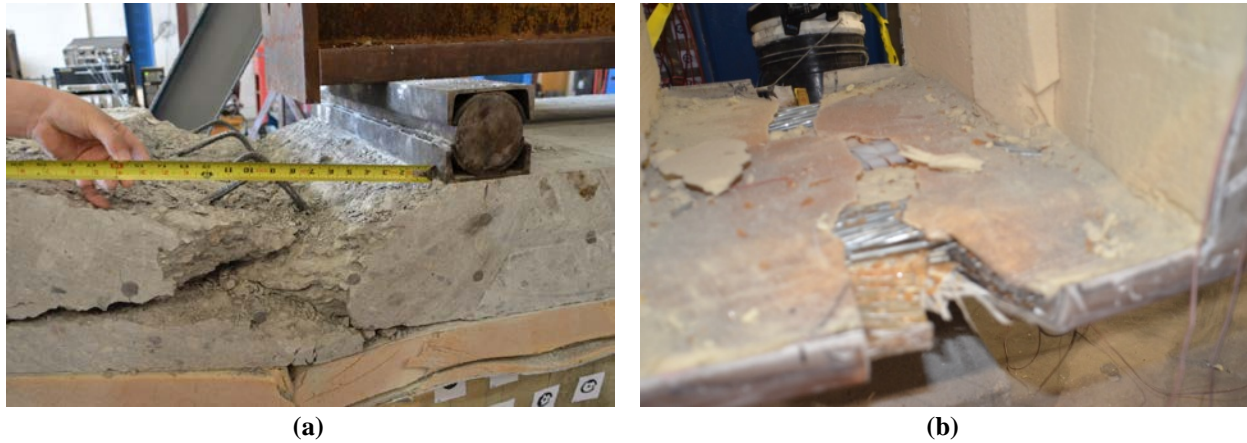
Figure 20. HCB Flexural Failure Modes: (a) Concrete Crushing in Undamaged HCB1; (b) Strand Delamination From FRP Shell in HCB2 With Imposed Damage


| (a) | (b) |
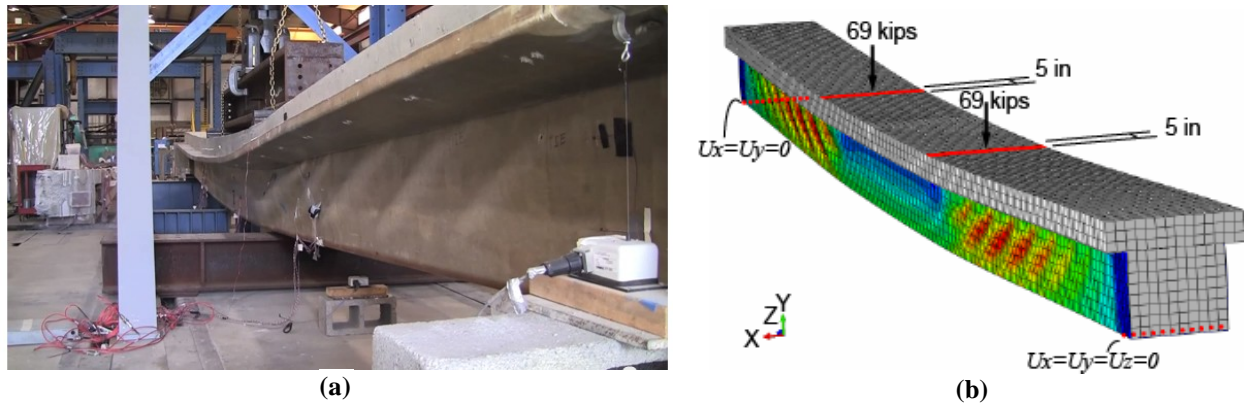
Figure 21. HCB1 FRP Shell Delaminates From the Foam Core Creating Shear Buckling Half-Waves in the Shear Span Near Ultimate Load: (a) Observation From Experiment; (b) Finite Element Simulation

Mid-span strain profiles through the HCB depth become increasingly nonlinear as moment increases in the undamaged HCB1 beam, as shown in Figure 22, with the neutral axis remaining relatively constant at approximately 22 in from the bottom fiber. For the damaged beam HCB2, the strain profile shows that bottom fiber strains are approximately 280% higher (compare 0.001 in/in to 0.0028 in/in at 300 kip-ft) than in the undamaged beam (HCB1) and high compressive strains in the concrete could not be developed.

The tested flexural capacities are lower than predictions calculated by assuming a force couple between the bridge decks and prestressing strands and ignoring the FRP shell; compare

20

1,035 kip-ft (tested) to 1,530 kip-ft (predicted) for HCB1 and 610 kip-ft (tested) to 720 kip-ft (predicted) for HCB2. For the undamaged HCB1, the strength prediction neglects the outer fiber concrete compressive strain amplification represented in the nonlinear strain profile near failure (see Figure 22a) caused by the FRP shell shear flexibility. For the damaged specimen, the prediction approach assumes failure occurs by steel strand yielding; however, in the test the strands debonded before they could yield. This debonding limit state should be considered when developing an HCB design guide, including provisions for the case when strand-shell bond is lost and the strand end anchorages are needed to maintain beam integrity.
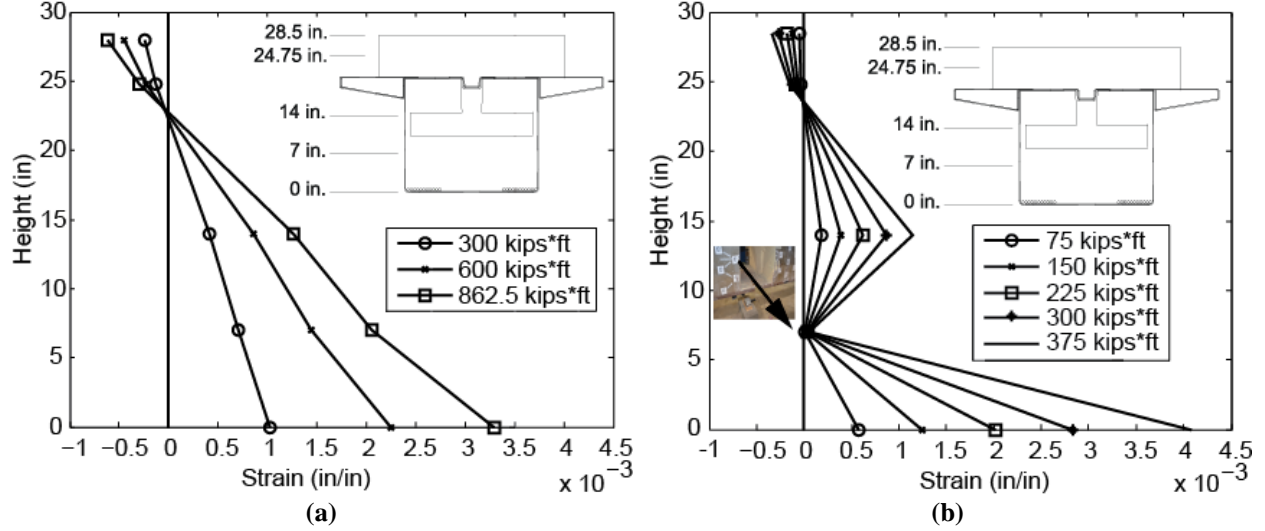
Figure 22. Mid-Span Strain Profile From the Phase 5 Ultimate Strength Tests for (a) HCB1 Without Damage and (b) HCB2 With Induced Damage

A shear design procedure was developed based on the ultimate strength test observations and finite element simulations shown in Figure 21b. The procedure assumes that shear at any HCB cross-section is carried by the FRP shell and the concrete arch and fin. The shear demand proportions are defined by the moments of inertia of the FRP shell and arch.

Concrete shear capacity is calculated with AASHTO equations ($\phi V_{n,concrete} \geq V_{u,concrete}$) and FRP shell shear capacity is defined by the FRP principal tensile strength along a shear buckling half-wave ($\phi V_{n,frp} \geq V_{u,frp}$). If either the factored FRP or the concrete capacity is less than the demand, then the HCB is assumed to fail in shear. Hypothesizing that the demand shear is distributed to the FRP and concrete components at any location along the beam based on respective transformed moments of inertia, then:

$$V_{u,frp} = (I_{frp}/I_{gross})V_u \qquad\qquad (1)$$

and

$$V_{u,concrete} = (I_{concrete}/I_{gross})V_u \qquad\qquad (2)$$

where

21

I_{frp} includes the prestressing strand transformed area
$I_{concrete}$ includes the concrete deck and fin and arch if it is not cracked.

Concrete shear capacity is assumed as:

$$V_{n,concrete} = V_{n,deck} + V_{n,fin} + V_{n,arch} + V_{Resal} \qquad (3)$$

where

$$V_n = 2(f'c)^{0.5}bd. \qquad (4)$$

The expression in Equation 4 for V_n is used for the bridge deck, arch and fin including the Resal effect (beneficial shear component from inclined arch compression) if the arch is helping (not cracked) at the shear ultimate limit state.

The FRP shell shear capacity is:

$$V_{n,frp} = min(V_{n,tie}, V_{n,strut}, V_{n,foam}). \qquad (5)$$

At a shear ultimate limit state, the FRP exhibits buckling half-waves as the shell delaminates from the foam. Tension field action carries a portion of the total demand shear ($V_{u,frp}$) to the support, as shown in Figure 23. Tension is carried along the half-wave peaks (tension tie: $V_{n,tie}$) and this tension is equilibrated with orthogonal compression struts ($V_{n,strut}$). Compression flows over the half-waves through the FRP. The half-wave acts as a short, braced column, where the bracing is provided by the interior foam ($V_{n,foam}$).
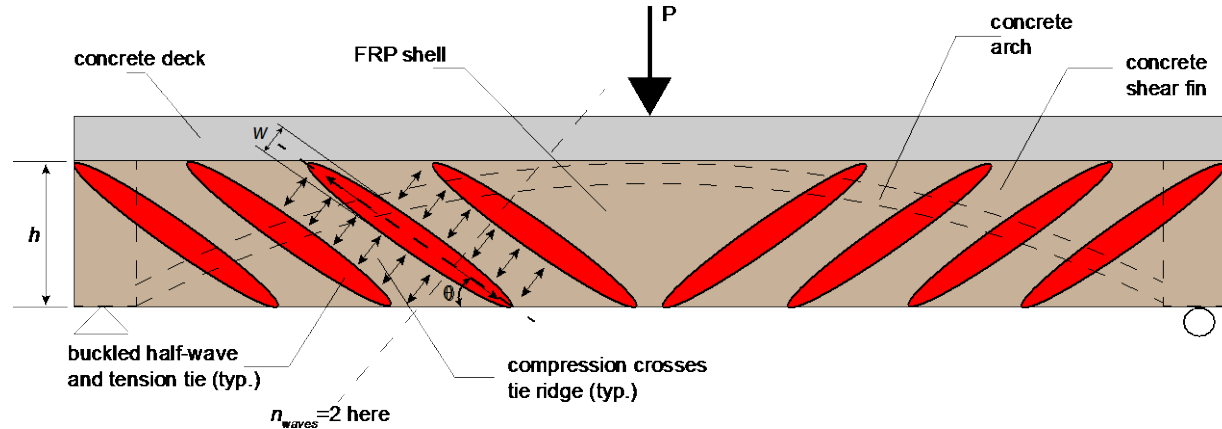

Figure 23. HCB Shear Behavior Including FRP Buckling and Tension Field Action

The tension tie capacity is:

$$V_{n,tie} = n_{webs} n_{waves} \sigma_{u,frp} \ twsin(\theta) \qquad (6)$$

where

t = FRP web wall thickness

22

θ = tie (half-wave) angle

n_{waves} = number of half-waves (ties) passing through the plane orthogonal to a half-wave

n_{webs} = number of FRP shell webs

$\sigma_{u,frp}$ = FRP ultimate tensile stress

$w = h\sin(\theta)/2$ is the tie width.

The compression strut capacity $V_{n,strut}$ is calculated with the Perry-Robertson column capacity formula (Trahair, 1993):

$$\sigma_{u,frp} = \frac{V_{n,strut}}{n_{webs}A_{strut}\sin\theta}\left(1 + \frac{\delta_o\left(\frac{t}{2}\right)}{\frac{I_{strut}}{A_{strut}}\left(1 - \frac{V_{n,strut}}{V_{cr,strut}}\right)}\right) \tag{7}$$

where

δ_o = the initial column geometric imperfection, assumed to be $w/1000$

$$I_{strut} = \frac{1}{12}\frac{h}{\sin\theta}t^3 \tag{8}$$

$$A_{strut} = \frac{ht}{\sin\theta} \tag{9}$$

$$V_{cr,strut} = \pi^2 E_{frp}I_{strut}/w^2. \tag{10}$$

Equation 7 is transcendental and $V_{n,strut}$ is solved for numerically, such as using the "Goal Seek" function in Microsoft Excel.

The foam compression capacity, $V_{n,foam}$, is calculated as

$$V_{n,foam} = \sigma_{y,foam}wh \tag{11}$$

where

$\sigma_{y,foam}$ is the foam yield stress.

Equation 11 is derived assuming the horizontal thrust in the FRP "column" (i.e., the compression strut across the tension tie in Figure 23) is equal to the pressure resultant on the foam.

CONCLUSIONS

Service

- *HCB FRP shell, steel strands, and concrete arch and bridge deck behave linear-elastically under service level live loads.*

- *The transformed area approach for calculating HCB section properties is valid for vertical deflection predictions.*

- *Before the bridge deck is placed, the HCB concrete arch is susceptible to local bending effects from point loads.*

- *Live load is distributed evenly in the HCB system when the edge stiffening effect of a traffic barrier is not taken into account.* Skew effects similar to those in the Tides Mill Stream Bridge have minimal effect on live load distribution factors for this type of system because the girders are relatively narrow and torsionally flexible. However, the presence of traffic barriers may influence the behavior of the superstructure.

Ultimate

- *The VDOT bridge deck strip design method, including the use of truss bars, is not applicable to this bridge type where plate behavior defines wheel load distribution to the beams.* Punching shear is a more applicable limit state. Furthermore, the deck appears to be supported primarily by the concrete fin, which dictates the span length for the deck design.

- *When in good condition, the flexural failure mode for an HCB structure will likely be concrete deck crushing. If an HCB has been damaged or is in poor condition, strand debonding is the likely failure mode.*

- *The FRP shell contributes to the flexural and shear capacity of the HCB when the beam is under composite live load.*

- *Accounting for outer fiber strain amplification from FRP shell shear deformation can improve HCB flexural strength predictions.*

- *The stiffness of the foam inside the FRP shell is fundamental to the beam shear strength at ultimate loads because it braces the shell webs, allowing tension field action to develop.*

RECOMMENDATIONS

1. *VDOT's Structure and Bridge Division should consider the HCB as an alternative in a value-engineering assessment, where the deck engineering should consider other design approaches instead of the strip method.* Highlighting the fact that this technology is a

proprietary design, experimental results confirmed that the HCB is viable for bridge construction and service, with low stresses and linear-elastic behavior under service live loads and high ductility and large flexural deformations observed before reaching a flexural limit state. However, the traditional strip method is inconsistent with observed local plate deformation behavior of the deck on top of the HCB system. Transverse bridge deck reinforcing could be reduced and truss bars eliminated if improved live load distribution models, such as calculating deck flexural demand and through-depth principal tensile stresses using plate theory, were implemented with careful consideration of early age concrete bridge deck shrinkage stresses. These shrinkage stresses are often much higher than live load service stresses. Furthermore, truss bars can potentially reduce transverse flexural capacity because the rebar placement does not correspond to tensile demand developed from plate behavior observed in both physical experiments and computer simulations.

2. *VDOT's Structure and Bridge Division should support the development of an AASHTO design guide for the HCB.* Components that should be incorporated into the guide include: transformed area for use in predicting deflections, a force couple in calculating flexural capacity, and tension field action for checking the shear capacity of the FRP shell. Additional research will be necessary for determining lateral load distribution factors.

IMPLEMENTATION AND BENEFITS

Implementation

1. *With regard to Recommendation 1, at this time, VDOT's Structure and Bridge Division is willing to consider the HCB superstructure system as an alternative for bridge construction and superstructure replacement projects on a case-by-case basis and when doing so to consider alternative deck design methodologies.* However, due to the proprietary nature of this technology, the division will not develop any standards for or perform any in-house design with this system. Furthermore, although the research in this report has shown that HCBs have the strength and ductility needed to support design loads, there are concerns about being able to inspect the components of these structures in service, particularly when traditional inspection methods are not necessarily effective. To that end, the Virginia Transportation Research Council (VTRC) has initiated a study that is investigating the durability of HCB components in marine exposures and will identify criteria and methods for in-service inspection. The study is anticipated to be complete by December 2018.

2. *With regard to Recommendation 2, although VDOT's Structure and Bridge Division is not internally developing standards specific to HCB technology, it will support such development through its participation in the AASHTO Subcommittee on Bridge and Structures (SCOBS).* This activity will be dependent upon SCOBS' priorities and does not have a fixed completion date.

Benefits

The benefit of implementing *Recommendation 1* is chiefly lower transportation costs, smaller construction equipment needs, and faster construction, which ultimately could lead to lower construction costs and shorter lane closures for the traveling public. The HCB is most suitable for short to medium spans (20 ft to 80 ft), although spans over 100 ft have been built. It was selected for the Tides Mill Stream site because the eight beams could be quickly placed with smaller, on-site construction equipment rather than larger cranes that would have been needed with a comparable system of eight 48-in-wide by 21-in-deep prestressed voided slabs. The fiberglass shell that surrounds the composite beams is also believed to offer higher resistance to the harsh marine environment at this site. Regardless of which beam designs were chosen, there would be a 7.5-in-thick cast-in-place bridge deck on top.

A key construction difference between the HCB and a precast concrete voided slab is site placement weight. Each HCB was filled with self-consolidating concrete at a local precasting plant and weighed 10,000 lb, as compared to 32,000 lb for a 48-in voided concrete slab. Lifting the heavier voided slab requires a larger crane (or multiple cranes) on site. As shown in Figure 24, however, the HCBs for the Tides Mill Stream Bridge were placed with a 100-ton capacity crawler, which was already on site because of the steel sheet pile cofferdams that were installed to rehabilitate the abutments.

Improved construction speed is also an advantage of the HCB system when compared to voided slabs. It is estimated based on contractor input that setting the voided slabs would have taken 3 to 4 days, primarily because only a single voided slab can be delivered per truck whereas three or four HCBs can be delivered at once. In addition, voided slab shear-key grouting and transverse post-tensioning would prevent deck rebar placement for 7 days after setting the slabs. On the other hand, the contractor placed all of the HCBs for the Tides Mill Stream Bridge in 1 day and began tying deck rebar immediately. This means that the HCB system saved more than 1 week of construction time for this project.

Figure 24. HCB Placement With 100-Ton Capacity Crawler Crane at Tides Mill Stream

The bid price of $29,500 for each HCB included a $2,500 design fee, delivery, and installation. For this particular project, the contractor requested that a local precaster place the concrete at their plant. Had the concrete been placed at the job site, the contractor could have saved $150 per beam in shipping. Thus, excluding the design fee, the installed cost per beam would have been reduced to $26,850. This cost compares to $16,000 per voided slab beam, based on a VDOT 2-year average cost for 40- to 50-ft spans. Because VDOT had predetermined they would use the HCB for this project, savings to the abutments due to the lighter superstructure were not determined. However, those additional savings could have been substantial, making the total project costs more comparable with those of conventional construction. Since this project was still early in the commercialization of the HCB, it is anticipated that HCB manufacturing costs will be reduced to make them first-cost competitive for future projects.

Supporting the development of a design guide, per *Recommendation 2*, will serve to provide more knowledge regarding the design of an HCB bridge, which will ultimately deliver a better quality product upon completion.

ACKNOWLEDGMENTS

REFERENCES

Ahsan, S. *Evaluation of Hybrid-Composite Beam for Use in Tide Mill Bridge.* Master's Thesis. Virginia Polytechnic Institute and State University, Blacksburg, 2012.

American Association of State Highway and Transportation Officials. *LFRD Bridge Design Specifications: Fourth Edition.* Washington, DC, 2008.

ASTM C39 / C39M-14a: Standard Test Method for Compressive Strength of Cylindrical Concrete Specimens. *Book of Standards, Volume 04.02.* ASTM International, West Conshohocken, PA, 2014.

ASTM C469 / C469M-14: Standard Test Method for Static Modulus of Elasticity and Poisson's Ratio of Concrete in Compression. *Book of Standards, Volume 04.02.* ASTM International, West Conshohocken, PA, 2014.

ASTM C496 / C496M-11: Standard Test Method for Splitting Tensile Strength of Cylindrical Concrete Specimens. *Book of Standards, Volume 04.02.* ASTM International, West Conshohocken, PA, 2004.

Bajzek, S. *Transverse Deck Reinforcement for Use in Tide Mill Bridge.* Master's Thesis. Virginia Polytechnic Institute and State University, Blacksburg, 2012.

Harris, D.K., and Civitillo, J.M. *In-Service Performance Evaluation and Monitoring of the Hybrid Composite Beam Bridge System on Route 205 Over Tides Mill Stream.* VTRC 18-R5. Virginia Transportation Research Council, Charlottesville, 2017.

Hillman, J.R. *Investigation of a Hybrid-Composite Beam System.* Final Report for High-Speed Rail IDEA Project 23. Transportation Research Board, Washington, DC, 2003.

Hillman, J.R. *Product Application of a Hybrid-Composite Beam System.* IDEA Program Final Report For the Period September 2003 through December 2007. Transportation Research Board, Washington, DC, 2008.

Kernicky, T.P., Whelan, M.J., and Moen, C.D. Influence of Prestressing Strand Damage on Modal Parameters of a Hybrid Composite Bridge Beam. *Proceedings of the IMAC XXXIII International Modal Analysis Conference*, Orlando, FL, 2015.

Maine Department of Transportation. *Knickerbocker Bridge Plans.* Augusta, 2009.

Mascaro, M., and Moen, C.D. *Out-of-Plane Web Deformation and Relative Arch Movement of Hybrid-Composite Beams Based on Photogrammetry.* Structural Engineering and Materials Report CE/VPI-ST-12/08. Virginia Polytechnic Institute and State University, Blacksburg, 2012.

Sasha N.B. *Transverse Deck Reinforcement for Use in Tide Mill Bridge.* Master's Thesis. Virginia Polytechnic Institute and State University, Blacksburg, 2013.

Snape, T., and Lindyberg, R. *Test Results: HC Beam for the Knickerbocker Bridge.* Advanced Structures & Composites Center, Orono, ME, 2009.

Simulia. *ABAQUS/Standard Version 6.12-1.* Dassault Systèmes, Providence, RI, 2014.

Van Nosdall, S. *Experiments on a Hybrid-Composite Beam for Bridge Applications.* Master's Thesis. Virginia Polytechnic Institute and State University, Blacksburg, 2013.

Van Nosdall, S., Moen, C.D., Roberts-Wollmann, C., and Cousins, T. Experiments on a Hybrid-Composite Beam for Bridge Applications. *Transportation Research Record: Journal of the Transportation Research Board,* No. 2332, 2013, pp. 43-52.

Virginia Department of Transportation. *Road and Bridge Standards.* Richmond, 2008.

Virginia Department of Transportation. *Manual of the Structure and Bridge Division.* Richmond, 2011.